

Optical properties of SiC nanotubes: A systematic *ab initio* study

I. J. Wu and G. Y. Guo*

*Department of Physics and Center for Theoretical Sciences,
National Taiwan University, Taipei, Taiwan 106, R.O.C.*

(Dated: November 30, 2018)

The band structure and optical dielectric function ϵ of single-walled zigzag [(3,0),(4,0),(5,0),(6,0),(8,0),(9,0),(12,0),(16,0),(20,0),(24,0)], armchair [(3,3),(4,4),(5,5),(8,8),(12,12),(15,15)], and chiral [(4,2),(6,2),(8,4),(10,4)] SiC-NTs as well as the single honeycomb SiC sheet have been calculated within density functional theory with the local density approximation. The underlying atomic structure of the SiC-NTs is determined theoretically. It is found that all the SiC nanotubes are semiconductors, except the ultrasmall (3,0) and (4,0) zigzag tubes which are metallic. Furthermore, the band gap of the zigzag SiC-NTs which is direct, may be reduced from that of the SiC sheet to zero by reducing the diameter (D), though the band gap for all the SiC nanotubes with a diameter larger than ~ 20 Å is almost independent of diameter. For the electric field parallel to the tube axis ($E \parallel \hat{z}$), the ϵ'' for all the SiC-NTs with a moderate diameter (say, $D > 8$ Å) in the low-energy region (0~6 eV) consists of a single distinct peak at ~ 3 eV. However, for the small diameter SiC nanotubes such as the (4,2),(4,4) SiC-NTs, the ϵ'' spectrum does deviate markedly from this general behavior. In the high-energy region (from 6 eV upwards), the ϵ'' for all the SiC-NTs exhibit a broad peak centered at ~ 7 eV. For the electric field perpendicular to the tube axis ($E \perp \hat{z}$), the ϵ'' spectrum of all the SiC-NTs except the (4,4), (3,0) and (4,0) nanotubes, in the low energy region also consists of a pronounced peak at around 3 eV whilst in the high-energy region is roughly made up of a broad hump starting from 6 eV. The magnitude of the peaks is in general about half of the magnitude of the corresponding ones for $E \parallel \hat{z}$. Interestingly, the calculated static dielectric constant $\epsilon(0)$ for all the SiC nanotubes is nearly independent of diameter and chirality with $\epsilon(0)$ for $E \parallel \hat{z}$ being only about 30 % larger than for $E \perp \hat{z}$. The calculated electron energy loss spectra of all the SiC nanotubes for both electric field polarizations are rather similar to that of $E \perp \hat{z}$ of the SiC sheet, being dominated by a broad $\pi + \sigma$ -electron plasmon peak at near 21 eV and a small π -electron plasmon peak at ~ 3 eV.

PACS numbers: 71.20.Tx, 73.22.-f, 78.67.Ch, 78.67.-n

I. INTRODUCTION

Since their discovery in 1991 [1], carbon nanotubes (CNTs) have attracted considerable interest worldwide because of their unusual properties and great potentials for technological applications. CNTs can be regarded as a layer of graphene sheet rolled up in a tubular form [2], and the structure of a CNT is specified by a chiral vector defined by a pair of integers (n, m). CNTs can be chiral or nonchiral depending on the way they are rolled up. Their physical properties, in particular, optical dielectric functions, depend sensitively on their chirality, i.e., the (n, m) indices (see, e.g., Ref. 3, 4 and references therein). Apart from CNTs, inorganic tubular materials, such as BN [5, 6], AlN [7], GaN [8], have also been predicted and synthesized. These tubular materials also display some very interesting properties distinctly different from their bulks.

Bulk silicon carbide (SiC) crystallizes in either a cubic or a hexagonal form, and exhibits polytypism [9, 10]. The polytypes are made of identical hexagonal layers with different stacking sequences. These polytypes are semiconductors with a range of band gaps, from 2.39 eV

in the zincblende (3C) to 3.33 eV in the wurtzite polytype (2H) [9, 11]. Furthermore, 3C and 6H SiC are used for high temperature, high-power and high-frequency devices [12, 13, 14, 15] due to their unique properties [16], while 6H SiC with a band gap of 2.86 eV is a useful material for blue light-emitting diode applications [11]. Recently, SiC-NTs were also synthesized by the reaction of CNTs and SiO at different temperature [17]. This has stimulated a number of both theoretical and experimental investigations on the tubular form of the SiC [18, 19, 20, 21, 22]. Based on density-functional calculations, Miyamoto and Yu [23] predicted the existence of graphitic and tubular forms of SiC and also proposed their synthesis using an extreme hole injection technique. They also reported that the strain energies of SiC-NTs are lower than that of CNTs, and that the band gaps of SiC-NTs can be direct or indirect, depending on the chirality. Using both tight-binding molecular dynamics and *ab initio* methods, Menon and coworkers [20] showed that single-walled SiC-NTs are highly stable with a large band gap. Zhao *et al.* [24] also investigated theoretically the strain energy, atomic and electronic structure of SiC-NTs with or without hydrogenation. Gali performed an *ab initio* study of the effect of nitrogen and boron impurities on the band structure of the SiC-NTs [25].

Unlike CNTs, SiC-NTs are polar materials and therefore, may exhibit some unusual physical properties that

*Electronic address: gyguo@phys.ntu.edu.tw

CNTs may not have. For example, zigzag SiC-NTs may become piezoelectric, and also show second-order non-linear optical response. Despite the intensive theoretical studies mentioned above, no *ab initio* calculation of the dielectric response and optical properties of SiC-NTs has been reported, perhaps because of the heavy demand on computer resources. A knowledge of the optical properties of SiC-NTs is important for their optical and electrooptical applications. The primary objective of this work is to analyze the band structure and optical characteristics of all three types of the SiCNTs by *ab initio* calculations. This will help to distinguish the electronic and optical properties of CNTs and BN-NTs from that of SiC-NTs. Our *ab initio* calculations are also needed to help understand the existing and future optical experiments.

This paper is organized as follows. In the next Sec., the theoretical approach and computational method are described. In Sec. III, the band structure, density of states (DOS), electron energy loss spectra (EELS), optical dielectric function of the single SiC sheet and SiC-NTs are discussed. Finally, conclusions are given in Sec. IV.

II. THEORY AND COMPUTATIONAL METHOD

Our *ab initio* calculations for the SiC-NTs are performed using the accurate full-potential projector augmented wave (PAW) method [26], as implemented in the VASP package. [27] They are based on density-functional theory (DFT) with the local-density approximation (LDA). The supercell method is used such that the identical SiC tubes are aligned in a square array and the closest interwall distance between the adjacent tubes is at least 10 Å. We consider a number of the SiCNTs with different diameters and chirality (n, m) from all three types, as listed in Table I.

First, the ideal SiC-NTs are constructed by rolling up a graphitic hexagonal SiC sheet. The atomic positions and lattice constants were then fully relaxed by the conjugate gradient (CG) method. The theoretical equilibrium atomic positions and lattice constant were obtained when the forces acting on all the atoms and the axial stress are less than 0.04 eV/Å and 1.0 kBar, respectively. In these atomic position optimizations, a uniform grid ($1 \times 1 \times n$) along the nanotube axis (z -axis) with the number n of the k -points being from 30 to 50. The special k -point method and the Gaussian broadening technique were used for the Brillouin zone (BZ) integration. The length of theoretical translational vector T and theoretical diameter D are listed in Table I. The curvature energy E_c (total energy relative to that of single SiC sheet) (also known as the strain energy) of the SiC-NTs is listed in Table II. Note that for the nanotubes with a moderate diameter (≥ 10 Å), the equilibrium structures are already found to be almost the same as that of the ideal nanotubes constructed by rolling-up a SiC sheet with a Si-C

TABLE I: Theoretical structural parameters of the SiC nanotubes studied. D is the diameter, T is the length of translational vector, and N is the number of atoms per cell.

	D (Å)	T (Å)	N
(3,3)	5.05	3.08	12
(4,4)	7.43	3.08	16
(5,5)	8.45	3.07	20
(8,8)	13.49	3.07	32
(12,12)	20.25	3.07	48
(15,15)	25.35	3.07	60
(3,0)	3.36	5.14	12
(4,0)	4.13	5.22	16
(5,0)	5.10	5.25	20
(6,0)	6.06	5.26	24
(8,0)	7.89	5.29	32
(9,0)	8.89	5.3	36
(12,0)	11.82	5.3	48
(16,0)	15.61	5.3	64
(20,0)	19.85	5.4	80
(24,0)	23.48	5.3	96
(4,2)	5.25	14.28	56
(6,2)	7.16	19.5	104
(8,4)	10.5	14.03	112
(10,4)	12.17	11.06	104

bondlength of 1.771 Å. This is consistent with the fact that the calculated E_c of the nanotubes with such a diameter is already smaller than 0.05 eV/atom (Table II). Interestingly, like CNTs and BN-NTs, the calculated E_c of the SiC-NTs can be very well fitted with $E_c = \alpha/R^2$ with $\alpha = 2.004$ eV·Å²/atom, indicating that the conventional elastic theory works well even down to such a small length scale. α for the SiC-NTs is identical to that of the CNTs but larger than that (1.248 eV Å²/atom) of the BN-NTs calculated previously using the same band structure method [5]. However, α of ~ 1.75 eV Å²/atom reported in Ref. 24 is somewhat smaller than the present calculations.

The final self-consistent electronic structure calculations were then performed on the theoretically determined structures of the SiC-NTs. In the self-consistent electronic structure calculations, the number n of the k -points along the z -axis used ranges from 40 to 50. The density of states (DOS) was evaluated from the final band structures by Gaussian broadening method:

$$N(\epsilon) = \sum_{n,\mathbf{k}} w_{\mathbf{k}} \delta(\epsilon - \epsilon_{n,\mathbf{k}}) \quad (1)$$

where the Dirac delta function $\delta(x)$ is approximated by the Gaussian function,

$$\delta(x) \approx \frac{1}{\sqrt{\pi}\Gamma} e^{-x^2/\Gamma^2}, \quad (2)$$

$w_{\mathbf{k}}$ is the weight associated with k -point \mathbf{k} , and $\epsilon_{n,\mathbf{k}}$ is the n th energy band. Here the Gaussian width Γ is set to 0.04 eV. A denser k -point grid along the z -axis with n ranging from 40 to 100 was used for the DOS calculations.

The optical properties were calculated based on the independent-particle approximation, i.e., the quasi-particle self-energy corrections, the local-field corrections and the excitonic effects were neglected. In particular, the band gap of SiC in the wurtzite (2H) structure from our LDA calculations is 2.15 eV, being 1.18 eV smaller than the experimental value [9, 11]. This suggests that the quasi-particle self-energy corrections to the optical peak positions may amount to ~ 1 eV in the SiC systems. Furthermore, because the LDA underestimates the energy gaps, the calculated dielectric function would be slightly too large in general. For example, our calculated dielectric function at 0 eV for the electric field parallel and perpendicular to the c -axis of 2H SiC is 8.33 and 7.90, respectively, being slightly larger than the corresponding measured ϵ_∞ , 6.84 and 6.51. [9] Therefore, the results from the present LDA-independent-particle calculations should not be quantitatively compared with experiments, though they would certainly be useful to study the trends and characteristics of the optical properties of the SiC-NTs. Nonetheless, our previous calculations show that the dielectric functions of graphite [3] and also of h-BN [5] calculated within the independent-particle picture are in reasonable agreement with experiments, perhaps because of the accidental cancellation of the self-energy corrections by the excitonic effects.

The imaginary part of the dielectric function $\epsilon(\omega)$ is given by the Fermi golden rule (see, e.g., Ref. 3) (atomic units are used in this paper), i.e.,

$$\epsilon''_{aa}(\omega) = \frac{4\pi^2}{\Omega\omega^2} \sum_{i \in VB, j \in CB} \sum_{\mathbf{k}} w_{\mathbf{k}} |p_{ij}^a|^2 \delta(\epsilon_{\mathbf{k}j} - \epsilon_{\mathbf{k}i} - \omega), \quad (3)$$

where ω is the photon energy and Ω is the unit cell volume. The dipole transition matrix elements $p_{ij}^a = \langle \mathbf{k}i | \hat{p}_a | \mathbf{k}j \rangle$ were obtained from the final self-consistent band structure with the PAW formalism. [28] VB and CB denote the valence and conduction bands, respectively. The $|\mathbf{k}n\rangle$ represents the n th Bloch state wave function with crystal momentum \mathbf{k} , and a represents the Cartesian component. We can obtain the real part of the dielectric function by the Kramer-Kronig transformation,

$$\epsilon'(\omega) = 1 + \frac{2}{\pi} \mathbf{P} \int_0^\infty d\omega' \frac{\omega' \epsilon''(\omega')}{\omega'^2 - \omega^2}, \quad (4)$$

where \mathbf{P} denotes the principal value of the integral. Given the complex dielectric function $\epsilon' + i\epsilon''$, all other linear optical properties such as reflectivity, refraction index, and absorption spectrum can be calculated. The electron energy loss spectra at the long wavelength limit is given by $-Im[(\epsilon' + i\epsilon'')^{-1}]$. The electric polarizability $\alpha(\omega)$ is defined by $\epsilon'(\omega) = 1 + 4\pi\alpha(\omega)/\Omega$.

In the present calculations, the δ -function in Eq. (3) is approximated by Gaussian function [Eq. (2)] with $\Gamma = 0.2$ eV. The same k -point grid as in the DOS calculations is used. As noticed before [3, 5], the unit cell volume Ω is not well defined for nanotubes. Therefore, as in previous calculations [3, 5], we used the effective unit cell volume

for the SiC-NTs instead of the volume of the supercells, which is arbitrary. The effective unit cell for a nanotube is given by $\Omega = \pi[(\frac{D}{2} + \frac{d}{2})^2 - (\frac{D}{2} - \frac{d}{2})^2]T = \pi DdT$, where d is the thickness of the SiC-NT cylinder which is set to the interlayer distance of h-SiC (3.51 Å). Although the value of the effective unit cell volume used may change the magnitude of the dielectric functions as can be seen from Eq. (3), it would not affect the energy positions and shapes in the dielectric functions.

III. RESULTS AND DISCUSSION

A. Single SiC sheet

In order to understand the calculated properties of the SiC-NTs, we have also calculated the self-consistent electronic band structure and dielectric function for an isolated honeycomb SiC sheet. The isolated SiC sheet is simulated by a slab-super-cell approach with an intersheet distance of about 10 Å. The underlying structure was determined theoretically by using a k -mesh of $10 \times 10 \times 1$, and the theoretical lattice constant is $a = 3.069$ Å.

The calculated band structure and density of states for the isolated SiC sheet are displayed in Fig. 1. Clearly, the SiC sheet is a semiconductor with a direct band gap of 2.58 eV. The top of valence bands and the bottom of conduction bands both occur at symmetry point K in the hexagonal Brillouin zone. Both the upper valence band and the lower conduction band are predominantly of Si and C p -orbital character. The upper valence band consists of one π band which arises from the $2p_z$ and $3p_z$ orbitals, extending above and below the SiC layer plane, and two σ bands involving the three Si $2s$, $2p_x$, $2p_y$ and three C $3s$, $3p_x$, $3p_y$ orbitals, which form the coplanar Si-C σ bonds. The low-lying conduction bands ranging from 2.4 eV to 5.6 eV are predominantly of the p_z character, indicating that they are the π^* bands. These electrons play an essential role for electrical conductivity.

The calculated dielectric function $\epsilon(\omega)$ of the SiC sheet is displayed in Fig. 1. In our calculations, a dense k -point grid of $60 \times 60 \times 1$ is used. The optical properties of the single SiC sheet can be roughly divided into two spectral region. In the low-energy range from 2 to 6 eV, the inter-band optical transitions involve mainly the π bands. At higher energies, the optical absorption peaks between 6 to 11 eV are associated with the interband transitions involving σ bands. Strong anisotropy in the optical spectra is expected due to distinct optical selection rules, as can be seen from Fig. 1. For a single SiC sheet, only $\pi \rightarrow \pi^*$ and $\sigma \rightarrow \sigma^*$ transitions are allowed if the electric field \vec{E} is polarized parallel to the SiC-layer plane ($E \parallel \hat{a}$). In contrast, only $\pi \rightarrow \sigma^*$ and $\sigma \rightarrow \pi^*$ transitions are allowed if the \vec{E} is polarized perpendicular to the SiC-layer plane ($E \perp \hat{a}$). This explains why there is a strong absorption peak at ~ 3.0 eV for ($E \parallel \hat{a}$) in the single SiC sheet [Fig. 1(c)]. For the single SiC sheet, there is no optical absorption for $E \parallel \hat{c}$ below ~ 5 eV (Fig. 1c).

The calculated electron energy loss spectra (EELS) of the SiC sheet are shown in Fig. 1e. For $E \parallel \hat{a}$, two prominent peaks are found in the energy loss function, $-Im\epsilon^{-1}$ (Fig. 1e). A small one at ~ 5 eV may be attributed to the collective excitation of π electrons partially screened by the σ electrons. A large broad resonance (actually, a multi-peak manifold) near 21.0 eV is associated with plasma oscillations involving both the π and σ electrons. For $E \parallel \hat{c}$, there is also a broad resonance in the high energy region, but at around 23.5 eV. However, there is no distinct peak at ~ 5 eV. There are instead many spiky thin peaks in the low energy region from 7 to 15 eV (Fig. 1e).

B. Band structure of the SiC nanotubes

The calculated band gaps of all the SiC-NTs are listed in Table II and also displayed as a function of the tube diameter in Fig. 2. The band structures of the selected zigzag, armchair and chiral SiC-NTs are shown in Figs. 3 and 4. All the SiC-NTs, with the exceptions of the ultrasmall (3,0) and (4,0) nanotubes, are semiconductors. In particular, all the semiconducting zigzag SiC-NTs have a direct band gap (Table II and Fig. 3). The top of valence bands and the bottom of the conduction bands both occur at the center (Γ) of the 1D Brillouin zone. This suggests that the zigzag SiC-NTs may find applications in optical and opto-electronic devices such as SiC lasers. Interestingly, the ultrasmall diameter zigzag (3,0) and (4,0) tubes are metallic (Fig. 3a-b and Table II). The (3,0) nanotube has a light electron pocket at Z with an effective mass of 0.27 and two doubly degenerate heavy hole pockets at Γ with an effective mass of 1.0. The (4,0) nanotube has a light electron pocket at Γ with an effective mass of 0.51 and two doubly degenerate heavy hole pockets at Z with an effective mass of 1.42. They could be the smallest SiC metallic nanowires and may have applications in nano-electronics and high efficient field emissions. Nevertheless, since the LDA underestimates the band gap, this prediction of metallic (3,0) and (4,0) zigzag SiC nanotubes should be treated with caution. In contrast, all the armchair and chiral SiC-NTs are indirect band gap semiconductors (see Table II and Figs. 4). For the armchair SiC-NTs, the bottom of conduction bands generally appears at the 1D Brillouin zone boundary (Z), while the top of valence bands occurs at somewhere between the Γ and Z points (Fig. 4).

Fig. 2 shows that the band gap of the small SiC-NTs increases with diameter, and approaches the band gap of the isolated SiC-sheet as the diameter becomes larger than ~ 20 Å. The reduction of the band gap in the small diameter SiC-NTs may be attributed to the curvature effects [29]. When a SiC sheet is rolled up to form a SiC-NT, the π and σ orbitals are no longer orthogonal to each other, and can hybridize. The hybridization of the π and σ orbitals would modify the band structures of the SiC-NTs obtained by rolling up a SiC-sheet. Re-

markably, the reduction of the band gaps of the zigzag SiC-NTs is monotonic and very large such that the ultrasmall (3,0) and (4,0) zigzag tubes become metallic (Fig. 2). This strong diameter dependence of the band gap can perhaps be used to engineer the band gap of the SiC-NTs by growing the tubes with a prespecified diameter. Nonetheless, the reduction of the band gap of the armchair SiC-NTs is much smaller (within 0.5 eV), except the (4,4) SiC-NT (Fig. 2). The reduction of the band gap for the chiral SiC-NTs is in between the zigzag and armchair nanotubes. A similar trend of the diameter dependence for the SiC-NTs was reported before in Ref. 21, though the sizes of the calculated band gaps reported in Ref. 21 are generally smaller than the ones presented here. This difference may be due to the fact that the different band structure calculation methods were used in the previous[21] and present calculations, namely, the linear combination of numerical atomic-orbitals method in Ref. 21 and the plane wave expansion method in this work. Apart from the differences in the band gaps, the calculated band dispersions in some SiC-NTs from Ref. 21 and this work differ noticeably too. For example, in Ref. 21, the bottom of the conduction bands of the (5,5) SiC-NT appears near the Γ point, while it occurs at the Z point in the present calculations. It is gratifying that the band dispersions of the (5,5) SiC-NT reported here (Fig. 4) is very similar to that in Ref. 23 obtained also using a plane wave expansion method.

We note that the electrical property of the CNTs depends strongly on their chirality. [2] For example, all the armchair CNTs are metallic. This is because the purely covalent honeycomb graphene sheet is a semimetal with the conduction and valence bands touching the K points in the hexagonal Brillouin zone. [2] In contrast, all the SiC-NTs except the ultrasmall diameter (3,0) and (4,0) nanotubes, are semiconductors. As pointed out by Zhao, *et al.*, [21] this is due to the ionicity of SiC which results in the opening of a band gap at the K points in the Brillouin zone of the honeycomb SiC sheet (Fig. 1). We also note that this diameter dependence of the band gap of the SiC-NTs (Fig. 2) is very similar to that found for the BN-NTs. [5] Nonetheless, the BN-NTs are insulators with a much wider band gap because of the much higher ionicity of the BN systems. [5, 6, 30]

C. Optical dielectric function of the SiC nanotubes

The calculated optical dielectric functions of some selected zigzag [(8,0), (9,0), (12,0), (16,0)], armchair [(4,4), (5,5), (12,12), (15,15)], chiral [(4,2), (8,4), (10,4)] SiC-NTs are shown in Figs. 5-7, respectively. The spectra can be roughly divided into two regions, namely, the low-energy one from ~ 2 to 6 eV and the high-energy one from 6 to 15 eV. Below about 2 eV (the band gap region), the ϵ'' is zero and ϵ' tends to a constant as the photon energy approaches zero. For the electric field parallel to the tube axis ($E \parallel \hat{z}$), the ϵ'' for all the three types of

TABLE II: Band gap E_g , band gap type, and curvature energy E_c [i.e., total energy relative to that of the SiC sheet (-7.68 eV/atom)] of the SiC nanotubes. The band gap of the single SiC sheet is 2.58 eV and direct.

	E_g (eV)	E_g type	E_c (eV/atom)
(3,3)	2.13	indirect	0.21
(4,4)	1.60	indirect	0.13
(5,5)	2.18	indirect	0.09
(8,8)	2.32	indirect	0.04
(12,12)	2.41	indirect	0.02
(15,15)	2.46	indirect	0.01
(3,0)	0(metal)	-	0.70
(4,0)	0(metal)	-	0.42
(5,0)	0.19	direct	0.26
(6,0)	0.70	direct	0.18
(8,0)	1.35	direct	0.11
(9,0)	1.53	direct	0.08
(12,0)	1.89	direct	0.05
(16,0)	2.15	direct	0.04
(20,0)	2.26	direct	0.02
(24,0)	2.35	direct	0.01
(4,2)	0.75	indirect	0.39
(6,2)	1.47	indirect	0.12
(8,4)	1.92	indirect	0.06
(10,4)	2.05	indirect	0.05

TABLE III: Static dielectric function $\epsilon(0)$, and polarizability $\alpha(0)$ per unit length of the SiC-NTs. The $\epsilon_{aa}(0)$ and $\epsilon_{cc}(0)$ of the single SiC sheet are 10.31 and 4.02, respectively.

	$\epsilon_{xx}(0)$	$\epsilon_{zz}(0)$	$\alpha_{xx}(0)$	$\alpha_{zz}(0)$
(4,4)	7.88	6.73	44.76	37.33
(5,5)	6.89	9.88	43.61	67.51
(8,8)	6.91	10.19	68.15	108.64
(12,12)	6.89	9.97	104.57	159.19
(15,15)	6.91	9.96	131.28	199.02
(3,0)	11.81	8.45	31.81	21.93
(4,0)	6.47	9.18	19.79	29.59
(5,0)	6.25	11.46	23.46	46.73
(6,0)	6.42	10.97	28.76	52.72
(8,0)	6.55	10.44	38.86	66.03
(9,0)	6.66	10.39	44.06	73.21
(12,0)	6.76	10.58	59.69	96.07
(16,0)	6.88	10.27	80.37	126.83
(20,0)	7.16	10.72	102.13	154.01
(24,0)	6.89	10.17	121.07	188.67
(4,2)	7.49	11.34	27.87	47.55
(6,2)	6.88	10.07	37.21	57.39
(8,4)	6.87	10.03	53.02	81.49
(10,4)	6.89	10.04	62.81	96.34

the SiC-NTs with a moderate diameter (say, $D > 9 \text{ \AA}$) in the low-energy region consists of a single distinct peak at $\sim 3 \text{ eV}$ plus a long shoulder of $\sim 2 \text{ eV}$ on the higher photon energy side (Figs. 5-7). This is very similar to the case of BN-NTs found in Ref. 5. Nonetheless, the peak in the SiC-NTs (Figs. 5-7) is about twice as high as that in the BN-NTs [5], because the BN-NTs have a band gap which is in general twice wide than that of the SiC-

NTs. However, this is in strong contrast to the case of CNTs in which the distinct features have been found especially for the semiconducting chiral nanotubes [3] and these features can be used to characterize the chirality of the grown carbon nanotubes by optical means [31, 32]. Nevertheless, for small diameter SiC nanotubes, the ϵ'' spectrum can deviate markedly from the general behavior described above (see Figs. 5-7). For example, for the armchair (4,4) nanotube, the pronounced peak at $\sim 3 \text{ eV}$ in the ϵ'' spectrum mentioned above is absent (Fig. 6a). For the chiral (4,2) nanotube, the pronounced peak in the ϵ'' spectrum shifts to low energy side by about 0.6 eV (Fig. 7a). In the high-energy region, the ϵ'' for all the types of the SiC-NTs have a broad peak of $\sim 6 \text{ eV}$ wide centered at $\sim 8 \text{ eV}$.

For the electric field perpendicular to the tube axis ($E \perp \hat{z}$), the ϵ'' spectrum of all the SiC-NTs except the small diameter nanotubes such as the (8,0) and (4,4), in the low energy region also consists of a pronounced peak at around 3.5 eV whilst in the high-energy region is, roughly, made up of a broad hump starting from 6.0 eV (Figs. 5-7). The magnitude of the peaks is in general about half of the magnitude of the corresponding ones for $E \parallel \hat{z}$, showing a moderate optical anisotropy in the SiC-NTs. In nanotubes, the electric field perpendicular to the nanotube axis is generally strongly screened [33, 34, 35, 36, 37], and this is known as the depolarization effect which is not taken into account in the present calculations. The depolarization effect may substantially reduce the magnitude of the ϵ'' spectrum for $E \perp \hat{z}$ [38], and hence enhance the optical anisotropy.

Let us now compare the optical dielectric function of the SiC-NTs with that of the single SiC sheet. It is clear from Fig. 1 and Figs. 5-7 that the ϵ'' spectrum for $E \parallel \hat{z}$ of the SiC-NTs is very similar to that of the single SiC sheet for $E \perp \hat{c}$. This is particularly true for the large or even moderate diameter SiC-NTs in which the curvature effect is small. This is perhaps not surprising because the electric field polarization is parallel to the SiC layer in both cases. However, the ϵ'' spectrum for $E \perp \hat{z}$ is rather different from that of $E \perp \hat{c}$ of the single SiC sheet. In particular, the ϵ'' spectrum for $E \perp \hat{c}$ for the photon energy below $\sim 5 \text{ eV}$ is zero in the single SiC sheet (Fig. 1), whilst in contrast, the ϵ'' spectrum for $E \perp \hat{z}$ of the SiC-NTs has a pronounced peak at $\sim 3.5 \text{ eV}$ (Figs. 5-7). This perhaps can be explained as follows. When $E \perp \hat{z}$, it is clear that for some parts of the tube wall, the electric field is nearly perpendicular to the SiC layer whilst for the other parts of the tube wall, it is roughly parallel to the SiC layer. Therefore, the dielectric function for $E \perp \hat{z}$ may be regarded as a mixture of the dielectric functions for both $E \perp \hat{c}$ and $E \parallel \hat{c}$ of single SiC sheet. This can be seen from inspection of Fig. 1 and Figs. 5-7, and is especially clear for the large diameter SiC-NTs. As a result, the calculated optical anisotropy of the large SiC-NTs is smaller than that of the single SiC sheet. Nevertheless, as mentioned before, the depolarization effect for $E \perp \hat{z}$ in the SiC-

NTs may considerably enhance the optical anisotropy of especially small diameter SiC-NTs. Therefore, in optical experiments, one may still see a rather strong optical anisotropy because the ϵ'' spectrum for $E \perp \hat{z}$ would be substantially reduced due to the depolarization effect.

D. Static dielectric response of the SiC nanotubes

The optical dielectric function $\epsilon(0)$ and electric polarizability $\alpha(0)$ in the zero frequency limit of the SiC-NTs are listed in Table III, and also displayed in Figs. 8 and 9. Note that the $\epsilon(0)$ [$\alpha(0)$] is the electronic contribution only [i.e., ϵ_∞ (α_∞)], and hence not the full static dielectric response [i.e., ϵ_{static} (α_{static})] which also contains the ionic contribution. In Ref. 37, it was found that including the ionic contribution would not change the observed trends, though the magnitude of the ionic contribution may be considerable.

Fig. 8 shows that to a first order approximation, the static dielectric constant $\epsilon(0)$ is almost a constant (i.e., independent of the diameter). The average value of $\epsilon(0)$ is 10.38 and 6.79 for $E \parallel \hat{z}$ and $E \perp \hat{z}$, respectively. The former is very close to $\epsilon_{aa}(0)$ of the single SiC sheet, while the latter is close to the circular average of the response of each part of the SiC-NT surface, which may be approximated by $0.5(\epsilon_{aa}(0) + \epsilon_{cc}(0))$ with quantities for the single SiC sheet (see Table III). Note that the static dielectric constants $\epsilon(0)$ of the SiC-NTs are about two times larger than that of the BN-NTs (~ 4.6 for $E \parallel \hat{z}$ and ~ 3.6 for $E \perp \hat{z}$) [5]. Therefore, the SiC-NTs may be better dielectric materials than the BN-NTs. It is clear from Fig. 8 that there is a pronounced anisotropy in the static dielectric response of the SiC-NTs. Interestingly, there is a small but discernable chirality dependent oscillation centered at the average value of $\epsilon(0)$ for both electric field polarizations. In particular, for $E \parallel \hat{z}$, the zigzag SiC-NTs have a slightly larger dielectric constant than the armchair ones.

The electric polarizability $\alpha(0)$ per unit length for both $E \parallel \hat{z}$ and $E \perp \hat{z}$ is proportional to the tube diameter D , as shown in Fig. 9. By fitting a linear function $\alpha(0) = a_0 D$ to the calculated $\alpha(0)$ -vs- D curves, we obtain a slope $a_{0,x} = 5.20$ for $E \perp \hat{z}$, and a slope $a_{0,z} = 7.81$ for $E \parallel \hat{z}$. As pointed out before for the BN-NTs [5], this linear relation between $\alpha(0)$ and D arises because the SiC-NTs are insulators in which the valence electrons are tightly bound to the ions and consequently, every atom of the same species has nearly the same static polarizability. Therefore, $\alpha(0)$ is proportional to the number of atoms per unit length which in turn is proportional to D . Nevertheless, the SiC-NTs exhibit a much stronger dielectric response than the BN-NTs since the BN-NTs have significantly smaller slopes ($a_{0,x} = 2.15$, $a_{0,z} = 3.04$). [5] This is because the SiC-NTs have a smaller band gap than the corresponding BN-NTs, as mentioned before.

Both the static dielectric constant $\epsilon(0)$ and electric polarizability $\alpha(0)$ are clearly anisotropic. The anisotropy

in electric polarizability can be best seen from the difference in the slopes between $E \parallel \hat{z}$ and $E \perp \hat{z}$, mentioned above. The $\alpha(0)$ for $E \parallel \hat{z}$ is about 50 % larger than that for $E \perp \hat{z}$. The actual anisotropy may be even larger because of the calculated $\epsilon(0)$ and $\alpha(0)$ for $E \perp \hat{z}$ would be reduced when the depolarization effect were taken into account.[34, 36, 37]

E. Electron energy loss spectrum

The calculated electron energy loss spectra of the zigzag, armchair and chiral SiC nanotubes are shown in Fig. 10. First of all, in the low energy region up to 15 eV, the EELS spectra for the all selected SiC nanotubes for both $E \parallel \hat{z}$ and $E \perp \hat{z}$ [except (4,4) tube for $E \parallel \hat{z}$] (Fig. 10), look very similar to that of $E \parallel \hat{a}$ of the SiC sheet (Fig. 1e). In particular, all the spectra have a rather pronounced π plasmon peak at ~ 5 eV and then the spectra grow steadily with energy. In the high energy region from 15 eV upwards, the spectra are dominated by a large broad $\pi + \sigma$ plasmon peak with the exact peak position being dependent on the chirality and also the electric field polarization. For the zigzag nanotubes, the energy position of the $\pi + \sigma$ plasmon peak is at ~ 22 eV for both electric field polarizations. For the chiral (4,2) and (8,4) nanotubes, respectively, the plasmon peak occurs at ~ 20 and ~ 22 eV for both $E \parallel \hat{z}$. For the armchair SiC nanotubes, the energy position of the $\pi + \sigma$ plasmon peak appears to oscillate around 21.5 eV (Fig. 10 c and d).

Surprisingly, there is only weak anisotropy in the EELS spectra for all the nanotubes (Fig. 10), in contrast to the rather pronounced anisotropy found in the dielectric functions (Figs. 5-7). The weak anisotropy in the EELS of the nanotubes may be attributed to the fact that for $E \perp \hat{z}$ all the $\pi \rightarrow \pi^*$, $\sigma \rightarrow \sigma^*$, $\pi \rightarrow \sigma^*$, and $\sigma \rightarrow \pi^*$ optical transitions are excited whilst the single SiC sheet only $\pi \rightarrow \pi^*$ and $\sigma \rightarrow \sigma^*$ transitions are possible for $E \parallel \hat{z}$.

IV. SUMMARY

An *ab initio* study of the structural, electronic and optical properties of the SiC-NTs within density functional theory in the local density approximation has been performed. In particular, the properties of the single walled zigzag [(3,0),(4,0),(5,0),(6,0),(8,0),(9,0),(12,0),(16,0),(20,0),(24,0)], armchair [(3,3),(4,4),(5,5),(8,8),(12,12),(15,15)], and chiral [(4,2),(6,2),(8,4),(10,4)] nanotubes have been calculated. For comparison, the electronic structure and optical properties of the single SiC sheet have also been calculated. We find that all the SiC nanotubes are semiconductors with exceptions of the ultrasmall (3,0) and (4,0) zigzag tubes which may be regarded as the thinnest conducting SiC nanowires. Interestingly,

the energy band gap of the zigzag SiC-NTs may be reduced from the full energy gap of the SiC sheet all the way down to zero by reducing the diameter (Fig. 2), though the band gap for all the SiC nanotubes with a diameter larger than ~ 20 Å approaches that of the SiC sheet. Furthermore, all the semiconducting zigzag SiC-NTs have a direct band gap. All these suggest that they may have interesting applications in optical and optoelectronic devices. Nonetheless, both the armchair and chiral SiC-NTs have an indirect band gap.

The optical properties of the SiC-NTs, as for the SiC sheet, can be divided into two spectral regions, namely, the lower energy region ($0\sim 6$ eV), in which the optical transitions involve mainly the π -bands, and the higher energy region from 6 eV upwards, where interband transitions involve mainly the σ -bands. For $E \parallel \hat{z}$, the ϵ'' for all the three types of the SiC-NTs with a moderate diameter (say, $D > 8$ Å for the zigzag SiC-NTs, $D > 6$ Å for the chiral SiC-NTs) in the low-energy region consists of a single distinct peak at ~ 3 eV. However, for the small diameter SiC nanotubes such as the (4,2),(4,4) SiC-NTs, the ϵ'' spectrum does deviate markedly from this general behavior. In the high-energy region, the ϵ'' for all the SiC-NTs exhibit a broad peak centered near 7 eV. For $E \perp \hat{z}$, the ϵ'' spectrum of all the SiC-NTs except the (4,4), (3,0) and (4,0) nanotubes, in the low energy region also consists of a pronounced peak at around 3 eV whilst

in the high-energy region is roughly made up of a broad hump starting from 6 eV. The magnitude of the peaks is in general about half of the magnitude of the corresponding ones for $E \parallel \hat{z}$, showing a moderate optical anisotropy in the SiC-NTs.

Interestingly, unlike the CNTs, the calculated static dielectric constant $\epsilon(0)$ for all the SiC nanotubes is almost independent of diameter and chirality with $\epsilon(0)$ for $E \parallel \hat{z}$ being only about 30 % larger than for $E \perp \hat{z}$. This is very similar to the case of the BN-NTs except that the values of $\epsilon(0)$ for the SiC nanotubes are about two times larger than that of the BN-NTs. The calculated electron energy loss spectra of all the SiC nanotubes studied here for both electric field polarizations are rather similar to that of $E \perp \hat{z}$ of the SiC sheet, being dominated by a broad $\pi + \sigma$ -electron plasmon peak at ~ 21 eV and a small π -electron plasmon peak at ~ 3 eV.

V. ACKNOWLEDGMENTS

The authors gratefully acknowledge financial supports from National Science Council, Ministry of Economic Affairs (92-EC-17-A-08-S1-0006) and NCTS of ROC. They also thank National Center for High-performance Computing of ROC for providing CPU time.

-
- [1] S. Iijima, Nature (London) **354**, 56 (1991).
 - [2] R. Saito, G. Dresselhaus, and M. S. Dresselhaus, Physical properties of Carbon Nanotubes(Imperial College, London, 1998).
 - [3] G. Y. Guo, K. C. Chu, D. S. Wang, and C. G. Duan, Phys.Rev. B **69**, 205416 (2004).
 - [4] G. Y. Guo, K. C. Chu, D. S. Wang, and C. G. Duan, Comput. Matter. Sci. **30**, 269 (2004).
 - [5] G. Y. Guo, J. C. Lin, Phys. Rev. B **71**, 165402 (2005).
 - [6] A. Rubio, J. L. Corkill, and M. L. Cohen, Phys. Rev. B **49**, 5801 (1994).
 - [7] M. Zhao, Y. Y. Xia, D. J. Zhang and L. M. Mei, Phys. Rev. B **68**, 235415 (2003).
 - [8] S. M. Lee, Y. H. Lee, Y. G. Hwang, J. Elsner, D. Porezag, and Th. Frauenheim, Phys. Rev. B **60**, 7788 (1999).
 - [9] von Münch, in *Landolt-Börnstein*, edited by O. Madelung, M. Schulz, and H. Weiss, New Series, Groups IV and III-V, Vol. 17, Pt. A (Springer, Berlin, 1982).
 - [10] R. W. G. Wyckoff, *Crystal Structures* (Wiley, New York, 1963).
 - [11] P. A. Ivanov and V. E. Chelnokov, Semicond. Sci. Technol. **7**, 863 (1992).
 - [12] C. Persson and U. Lindefelt, J. App. Phys. **82**, 5496, (1997)
 - [13] R. Wang, D. Zhang, C. Liu, Chemical Phys. Lett. **411**, 333, (2005).
 - [14] R. Rurali, P. Godignon, J. Rebollo, E. Hernandez, and P. Ordejon, Appl. Phys. Lett. **82**, 4298 (2003).
 - [15] C. H. Park, B. H. Cheong, K. H. Lee, and K.J. Chang, Phys. Rev. B **49**, 4485, (1994)
 - [16] *Properties of Silicon Carbide* edited by G. L. Harris (INSPEC, Institution of Electrical Engineers, London,1995)
 - [17] X.-H. Sun, C.-P. Li, W.-K. Wong, N.-B. Wong, C.-S. Lee, S.-T. Lee, and B.-K. Teo, J. Am. Chem. Soc. **124**, 14464 (2002).
 - [18] L. Z. Pei, Y. H. Tang, Y. W. Chen, C. Guo, X. X. Li, Y. Yuan, and Y. Zhang, J. Appl. Phys. **99**, 114306 (2006).
 - [19] L. Z. Pei, Y. H. Tang, X. Q. Zhao, Y. W. Chen and C. Guo, J. App. Phys. **100**, 046105 (2006).
 - [20] M. Menon, E. Richter, A. Mavrandonakis, G. Froudakis, and A. N. Andriotis, Phys. Rev. B **69**, 115322 (2004).
 - [21] M. Zhao, Y. Xia, F. Li, R. Q. Zhang and S. T. Lee, Phys.Rev. B **71**, 085312 (2005).
 - [22] A. Mavrandonakis, G. E. Froudakis, M. Schnell, and Muhlhauser, Nano Lett. **3**, 1481 (2004).
 - [23] Y. Miyamoto and B. D. Yu, Appl. Phys. Lett. **80**, 586 (2002).
 - [24] M. Zhao, Y. Xia, R. Q. Zhang, and S. T. Lee, J. Chem. Phys. **122**, 214707 (2005).
 - [25] A. Gali, Phys. Rev. B **73**, 245415 (2006).
 - [26] P. E. Blöchl, Phys. Rev. B **50**, 17953 (1994); G. Kresse and D. Joubert, *ibid.* **59**, 1758 (1999).
 - [27] G. Kresse and J. Hafner, Phys. Rev. B **47**, R558 (1993); **49**, 14251 (1994); G. Kresse and J. Furthmüller, Comput. Mater. Sci. **6**, 15 (1996).
 - [28] B. Adolph, J. Furthmüller, and F. Bechstedt, Phys. Rev. B **63**, 125108 (2001).
 - [29] S. Okada, S. Saito, and A. Oshiyama, Phys. Rev. B **65**, 165410 (2002).
 - [30] X. Blase, A. Rubio, S. G. Louie, and M. L. Cohen, Eu-

- rophys. Lett. **28**, 335 (1994).
- [31] S.M. Bachilo, M.S. Strano, C. Kittrell, R.H. Hauge, R.E. Smalley, and R.B. Wiesman, *Science* **298**, 2361 (2002).
- [32] Z.M. Li, Z.K. Tang, H.J. Liu, N. Wang, C.T. Chan, R. Saito, S. Okada, G.D. Li, J.S. Chen, N. Nagasawa and S. Tsuda, *Phys. Rev. Lett.* **87**, 127401 (2001).
- [33] H. Ajiki and T. Ando, *Physica B* **201**, 349 (1994); *Jpn. J. Appl. Phys., Suppl.* **34**, 107 (1995).
- [34] L. X. Benedict, S. G. Louie, and M. L. Cohen, *Phys. Rev. B* **52**, 8541 (1994).
- [35] A.G. Marinopoulos, L. Reining, A. Rubio, and N. Vast, *Phys. Rev. Lett.* **91**, 46402 (2003).
- [36] B. Kozinsky and N. Marzari, *Phys. Rev. Lett.* **96**, 166801 (2006).
- [37] G. Y. Guo, S. Ishibashi, T. Tamura and K. Terakura, *Phys. Rev. B* **75**, 245403 (2007).
- [38] A. G. Marinopoulos, L. Wirtz, A. Marini, V. Olevano, A. Rubio, and L. Reining, *Appl. Phys. A* **78**, 1157 (2004).

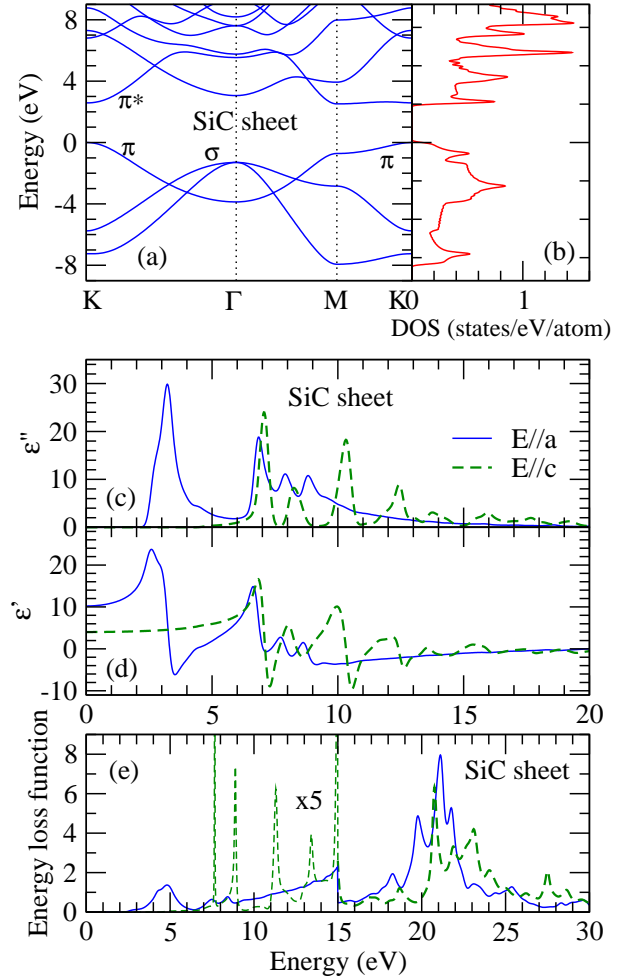


FIG. 1: (color online) Band structure, density of states (DOS), dielectric function and energy loss spectrum of the SiC sheet. In (a), the zero energy is at the top of the valence band. In (e), the spectra below 15 eV has been multiplied by five.

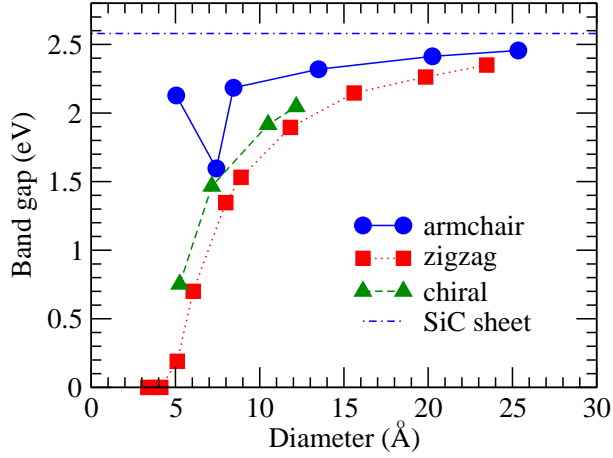


FIG. 2: (color online) Calculated band gaps of the SiC nanotubes vs diameter. For comparison, the band gap of the SiC sheet is shown as the dash-dotted line.

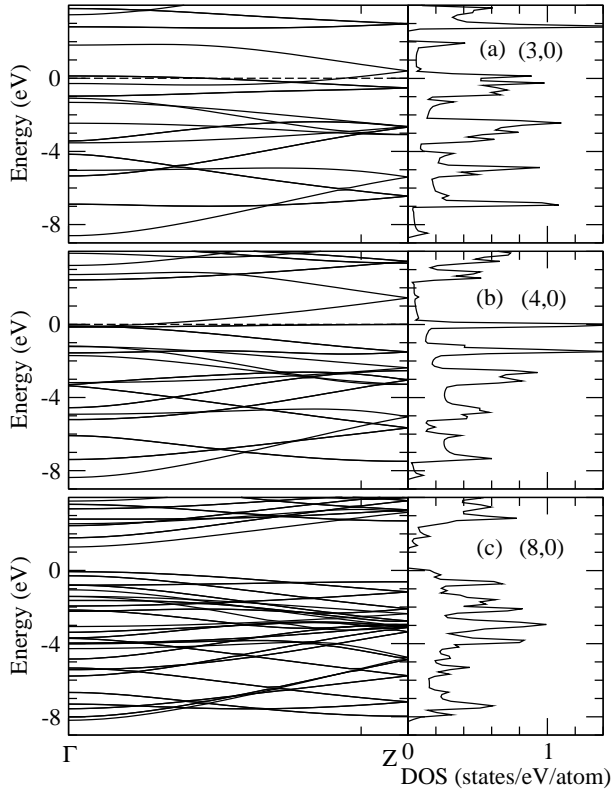


FIG. 3: Energy bands and density of states of the zigzag (3,0),(5,0) (8,0) SiC nanotubes. ΓZ is the 1D Brillouin zone of length π/T where T is the lattice constant (Table I). In (a) and (b), the dashed line indicates the Fermi level (0 eV). In (c) the top of the valance band is at 0 eV.

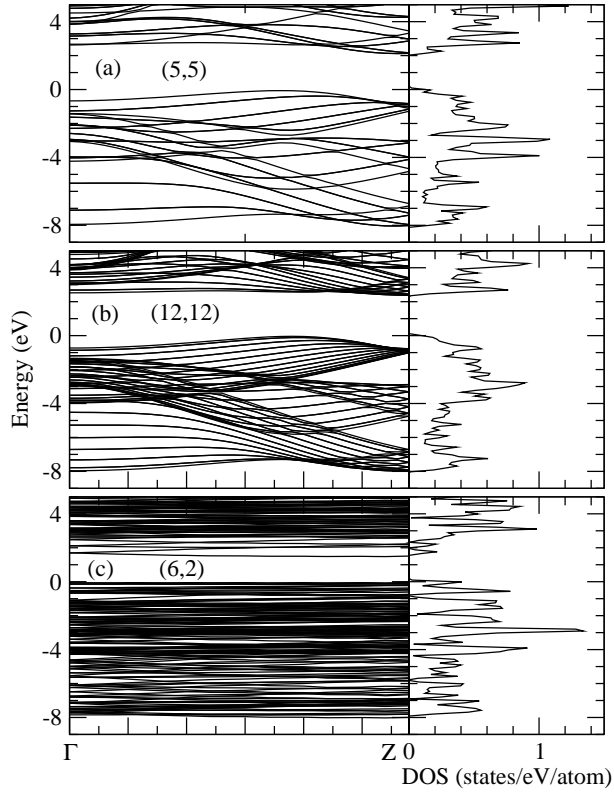


FIG. 4: Energy bands and density of states of the armchair (8,8), (12,12) and chiral (6,2) SiC nanotubes. The top of the valence band is at 0 eV. ΓZ is the 1D Brillouin zone of length π/T where T is the lattice constant (Table I).

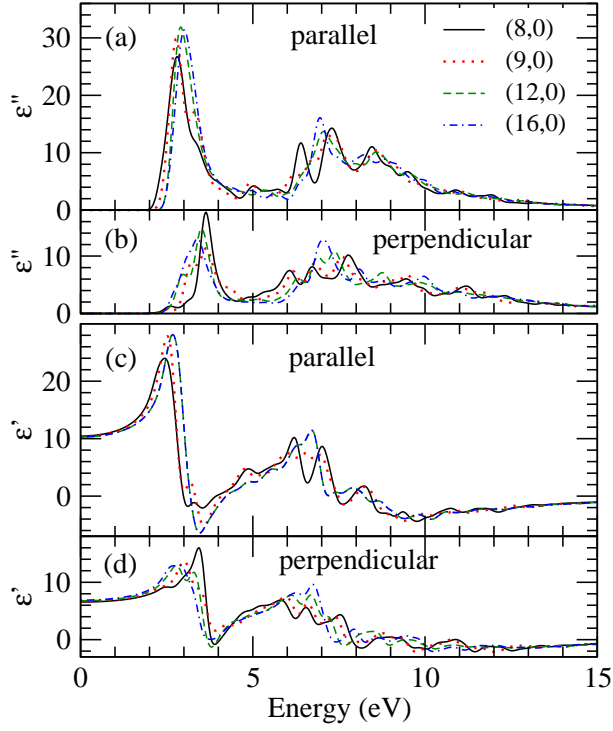


FIG. 5: (color online) Calculated dielectric functions of the zigzag SiC nanotubes. "Parallel" and "perpendicular" represent the electric field polarized parallel and perpendicular to the tube axis, respectively.

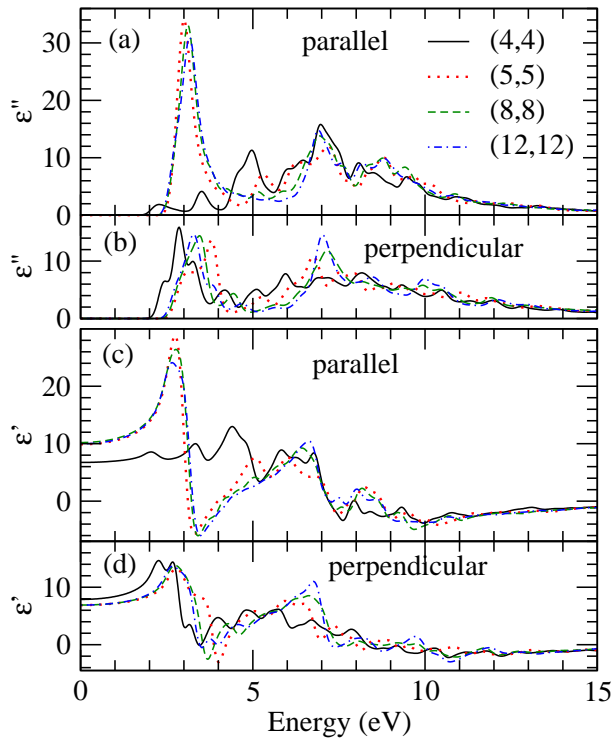


FIG. 6: (color online) Calculated dielectric functions of the armchair SiC nanotubes. "Parallel" and "perpendicular" represent the electric field polarized parallel and perpendicular to the tube axis, respectively.

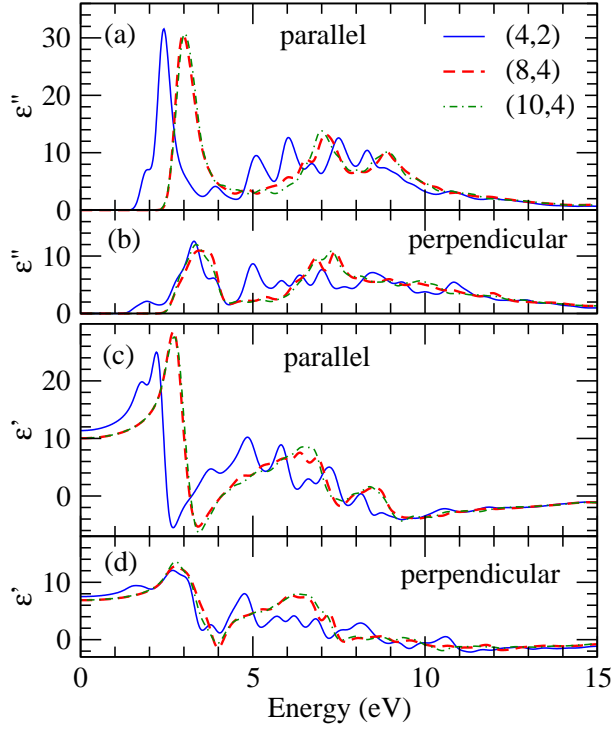


FIG. 7: (color online) Calculated dielectric functions of the chiral SiC nanotubes. "Parallel" and "perpendicular" represent the electric field polarized parallel and perpendicular to the tube axis, respectively.

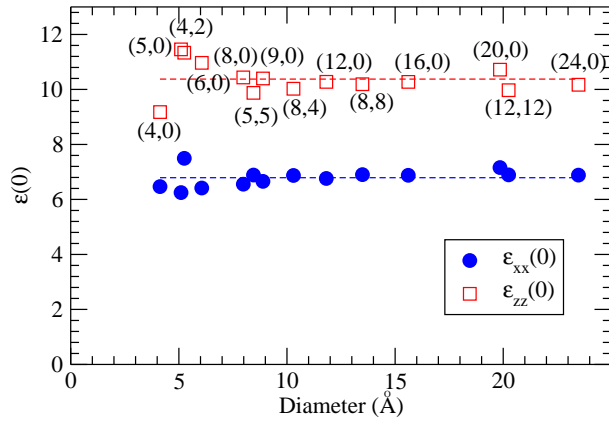


FIG. 8: Static dielectric constant $\epsilon(0)$ of the SiC nanotubes as a function of diameter. The dashed line is a constant least-squares fit.

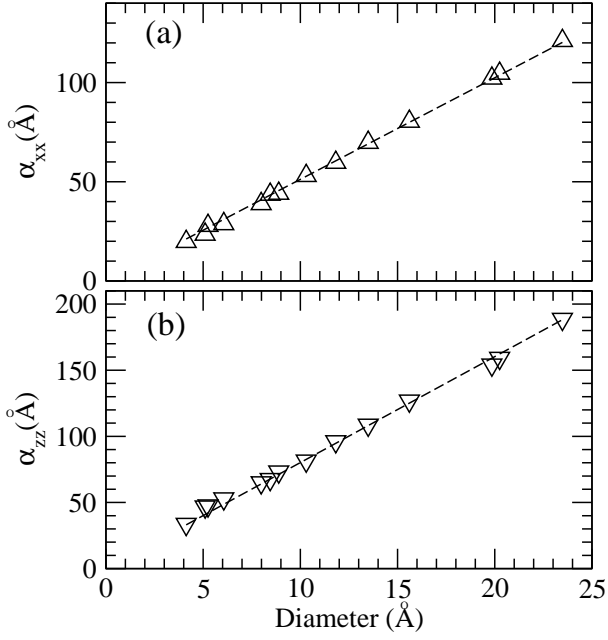


FIG. 9: (a) $\alpha_{xx}(0)$ and (b) $\alpha_{zz}(0)$ vs diameter D for the SiC nanotubes. The dashed line is a linear least-squares fit.

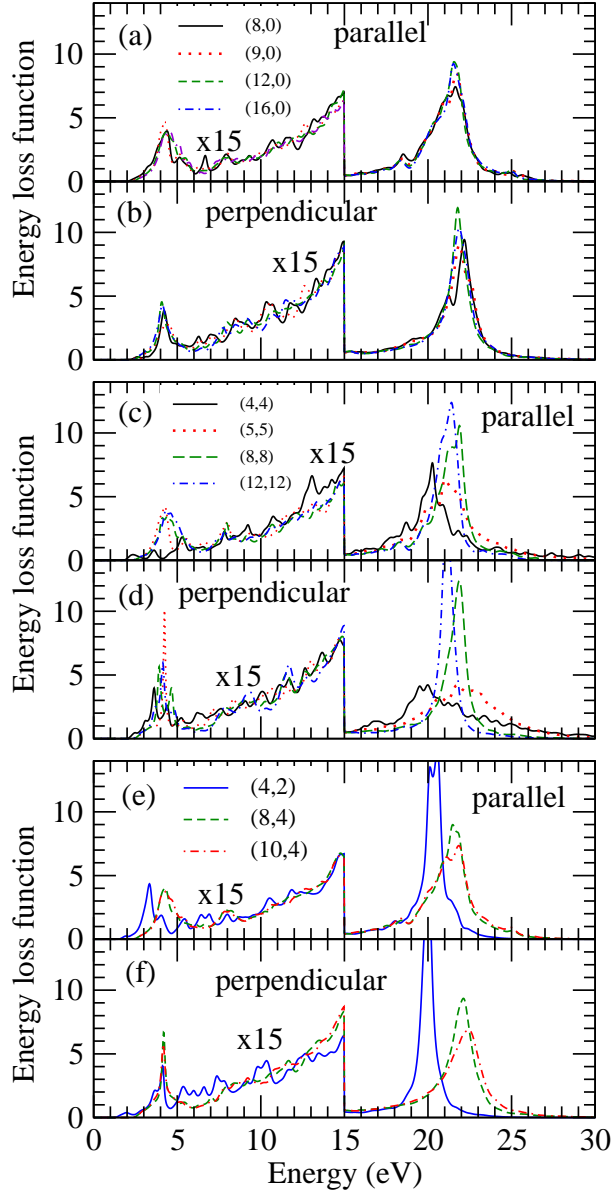


FIG. 10: (color online) Calculated energy loss function of the selected zigzag, armchair and chiral SiC nanotubes. "Parallel" and "perpendicular" denote the electric field polarized parallel and perpendicular to the tube axis, respectively.